The Astrophysical Journal Letters, 890:L21 (7pp), 2020 February 20 https://doi.org/10.3847/2041-8213/ab7348

Excitation Sources of Oscillations in Solar Coronal Loops: A Multi-wavelength Analysis

Sandra M. Conde C.[1,2], Rekha Jain[3], and Vera Jatenco-Pereira[1]
[1] Instituto de Astronomia, Geofísica e Ciências Atmosféricas, Universidade de São Paulo, Rua do Matão 1226, São Paulo, SP, 05508-090, Brazil
[2] School of Mathematics and Statistics, University of St. Andrews, St. Andrews KY16 9SS, UK
[3] School of Mathematics and Statistics, University of Sheffield, Sheffield S3 7RH, UK; R.Jain@sheffield.ac.uk
Received 2019 September 18; revised 2020 February 3; accepted 2020 February 3; published 2020 February 18

Abstract

An investigation into the excitation sources of oscillations detected in a coronal loop structure is carried out using the images obtained with *Interface Region Imaging Spectrometer* (*IRIS*) and the Atmospheric Imaging Assembly (AIA) instrument on board the *Solar Dynamics Observatory* (*SDO*). A loop structure in the active region AR 11967 on 2014 January 28, oscillating in the vicinity of a strong eruption and an M3.6 class flare site, is clearly noticeable in *SDO*/AIA 171 Å images. We study in detail, the oscillations with detected periods between 4 and 13 minutes and their connection in *IRIS* SJI 1330 Å and *SDO*/AIA 1700 Å images; both of these wavelengths sample the lower parts of the solar atmosphere. The simultaneous presence of many oscillations in the region of interest in all three wavelength passbands suggest that these oscillations were excited in the lower-chromosphere–photosphere plasma connected to the loop structure and then propagated at higher heights. We further investigate the Doppler velocity measurements from the spectrograph snapshots in *IRIS* C II 1336 Å, Si IV 1403 Å and Mg II k 2796 Å. These show signatures of upflows in the vicinity of the loop structure's endpoints estimated from 171 Å images. We suggest that some of the oscillations observed in AIA 171 Å have been triggered by plasma ejections and perturbations seen in the lower layers of the solar atmosphere. Based on the estimated phase speeds, the oscillations are likely to be slow magnetoacoustic in nature.

Unified Astronomy Thesaurus concepts: Solar physics (1476); Solar atmosphere (1477); Solar corona (1483)

Supporting material: tar.gz files

1. Introduction

Oscillations and waves play an important role in the study of the structure and dynamics of solar coronal loops. During a transient phase, it is not uncommon to see flaring events, and the oscillations in the nearby coronal loops in response to a flare. The waves and oscillations can be observed during several stages of the flare, in different wavelength bands, and can have periods from few seconds to several minutes (Aschwanden et al. 1999; Nakariakov et al. 1999, 2010; Verwichte et al. 2009; Kupriyanova et al. 2010; Kumar et al. 2016). It is interesting to analyze waves and plasma properties of the loops to understand the wave generation mechanisms in the solar corona (Jain et al. 2015; Allian et al. 2019). Although the Atmospheric Imaging Assembly (AIA; Lemen et al. 2012) on board the *Solar Dynamics Observatory* (*SDO*; Pesnell et al. 2012) allows us to observe oscillatory phenomena in coronal loops during transient events (Aschwanden & Schrijver 2011; Conde et al. 2016), the *Interface Region Imaging Spectrograph* (*IRIS*; DePontieu et al. 2014) data can allow us to see characteristics of the Transient Region and Chromosphere where we can search for the source of oscillations observed in the corona. The solar transition region is the interface between the chromosphere and the corona within which the temperature rapidly rises from 25,000 K to 1 MK.

In this work, we study oscillations in a coronal loop structure in the active region AR 11967 on 2014 January 28. We detected oscillations with periods 4, 6, 9, and 13 minutes from images taken with *SDO*/AIA instruments in 171 and 1700 Å band passes and also other periodicities in the SJI 1330 Å from *IRIS* instruments. *SDO*/AIA instruments provide images of the solar atmosphere with 0.6″ spatial resolution and 12 and 24 s of temporal cadence (Lemen et al. 2012). The SJI 1330 Å line is one of the far-ultraviolet (FUV) wavelength bands of *IRIS* that observes, with a spectral sampling of ∼13 mÅ pixel^{-1}, the chromospheric and strong continuum emission (see DePontieu et al. 2014). The oscillations were detected during the time when an M3.6 class flaring activity was recorded by the *Geostationary Operational Environmental Satellite* (*GOES*) instrument (Aschwanden 1994) in the active region. We investigate if these oscillations were linked at different heights in the solar atmosphere. We report for the first time the connection between oscillations with multiple periods detected in images of subarcsecond scales at different heights in the solar atmosphere. Such investigations give us the information on the driving mechanism of the coronal loop oscillations often seen in 171 Å coronal imagery.

The Letter is organized as follows. In Section 2 we present a description of the analyzed data and the method for detecting the periodicities. In Section 3 we present the results, followed by the Discussion and Conclusions in Section 4.

2. Observational Data and Analysis

We investigate intensity variations seen in the coronal loop structure of the active region AR 11967, which was on the southeast limb on 2014 January 28. The variations are obtained from the 171 Å images taken by *SDO*/AIA instrument with temporal cadence of 12 s and spatial resolution of 0.″6 per pixel. We also analyze in detail a smaller region of AR 11967 for which the aligned images were also available in *SDO*/AIA's 1700 Å spectral line and independently in NASA's *IRIS* in SJI 1330 Å spectral line.

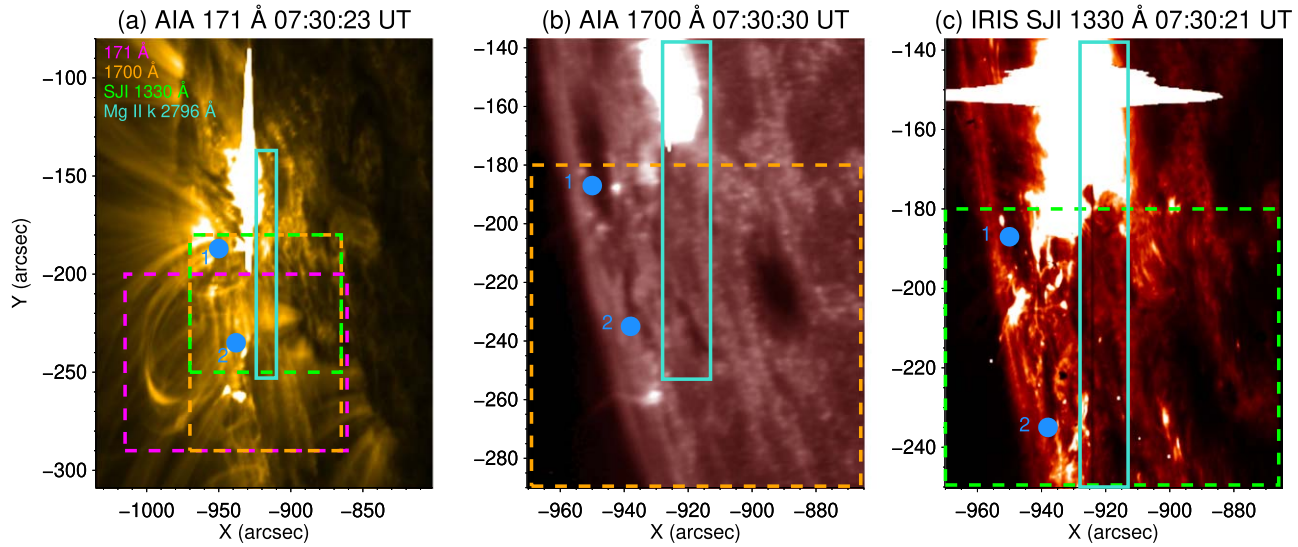

Figure 1. Image of AR 11967 on 2014 January 28 at about 07:30 UT observed in (a) *SDO*/AIA 171 Å (b) *SDO*/AIA 1700 Å and (c) *IRIS* SJI 1330 Å wavelength passbands. The orange dashed box on the left panel denotes the region of interest (ROI) of *SDO*/AIA 1700 Å images analyzed. The *IRIS* SJI 1330 Å data is available for a shorter region and is denoted by the green dashed box. The aquamarine box represents the region of interest (ROI) of spectral data (SG). The ROI chosen for the subsequent analysis includes the green, orange, and purple dashed lines. We indicate the position of the endpoints of the loops, as inferred from the 171 Å images, by the blue circle. Endpoint 1 is very close to the sunspot shown in 1700 Å (panel (b)).

The *IRIS* SJI 1330 Å images have a temporal cadence of 19 s and we co-aligned them, using correlation methods, with *SDO*/AIA 1700 Å images, which have a temporal cadence of 24 s. The *IRIS* SJI 1330 Å line is one of the strongest resonance lines in the solar ultraviolet spectrum (Rathore et al. 2015), which is believed to be formed in the solar region between the lower chromosphere and the transition region where as the *SDO*/AIA 1700 Å samples the solar region of temperature minimum to the photosphere.

We processed the *SDO*/AIA level 1 and *IRIS* level 2 data using aia_prep.pro and read_iris_l2.pro, respectively. We then co-aligned the data between both instruments using correlation methods.

We also considered the Mg II k 2796 Å, C II 1336 Å and Si IV 1403 Å lines of the raster files obtained from the spectrograph (SG) channels of *IRIS*. These files were multiple-repeat raster, with a field of view (FOV) of $14'' \times 19''$, in steps of $8'' \times 2''$ and temporal cadence for each step of 10.4 s. We carried out the wavelength calibration using iris_prep_wavecorr_l2.pro available in the Solar software.

Figure 1(a), displays a time snapshot of the extreme ultraviolet (EUV) image taken by the *SDO*/AIA instrument in 171 Å passband, where we can see the coronal loop analyzed in this work inside the purple dashed-line box. The FOV of the available data set in 1700 Å and SJI 1330 Å is shown in panel (b) and (c), respectively. We indicate these regions in panel (a) with the green and orange dashed boxes. In the same way, we show the FOV of the recorded raster data for Mg II k 2796 Å, C II 1336 Å and Si IV 1403 Å spectral lines, with the aquamarine box. We designate the points $1 = (-950'', -187'')$ and $2 = (-938'', -235'')$ as the *endpoints* of the loops as seen in 171 Å images and denote them with the blue filled-circle. The position of endpoint 1 is very close to a sunspot as can be seen in Figure 1(b).

We analyzed the AIA 171 Å images of the active region AR 11967 taken between 07:00 and 08:07 UT. During this observational time, an M3.6 flare (S10E75) was recorded with the enhancement in the X-ray flux by *GOES*-15 instrument from 07:25 to 07:34 UT. In addition to the flare, other eruptive activities[4] were also noted: jet-like features were seen in the vicinity of the endpoint 2, a coronal mass ejection between 07:00 and 10:00 UT, a short eruption from 06:50 to 06:54 in the coordinates $(-920.64'', -320.12'')$, which is close to endpoint 2, and another eruption close to the endpoint 1 $(-1026'', -217''.2)$ from 06:59:28 to 07:39:28 UT. It is also clear from the movies of *SDO*/AIA 171 and 304 Å images that we created (ar2.mp4 and ar304.mp4, respectively),[5] that there are eruptions close to the endpoint 1 around the same time as the M3.6 flare.

In order to minimize the saturation due to the flaring activity, we reduced the FOV on the images, referred to as the ROI for the subsequent analysis. At the same time, we would like to investigate the perturbations at the endpoint 1 and hence the ROI for *IRIS* SJI 1330 Å, the *SDO*/AIA 1700 and 171 Å are slightly different depending on the availability of data.

2.1. Method to Detect Waves

We prepared three-dimensional (3D) cubes (x, y, t) for *SDO*/AIA for 171 and 1700 Å from 07:00 to 08:07 UT. Similarly, we also considered 3D data cubes with *IRIS* SJI 1330 Å images between 7:30 and 8:07 UT, the only times for which data are available. In order to identify the periodicities present in the ROI, we calculated the Fast Fourier Transform (FFT) and Wavelet Transform[6] (Torrence & Compo 1998) of the temporal signal. The left column in Figure 2 shows the FFT power as a function of frequency (mHz) for 1700 Å (a) 171 Å (d) and 1330 Å (g) wavelengths. Peaks highlighted with a red asterisk indicate dominant periods present in the signal. In 1700 Å (a) and 171 Å (d) we have peaks at 6, 9, and 13 minutes. In 1330 Å

[4] Movies are available on the web pages of iSolSearch and Helioviewer http://www.lmsal.com/isolsearch and https://www.helioviewer.org, respectively.
[5] Movies ar2.mp4 and ar304.mp4 are available in the tar.gz package.
[6] Wavelet Transform software is available at http://paos.colorado.edu/research/wavelets/.

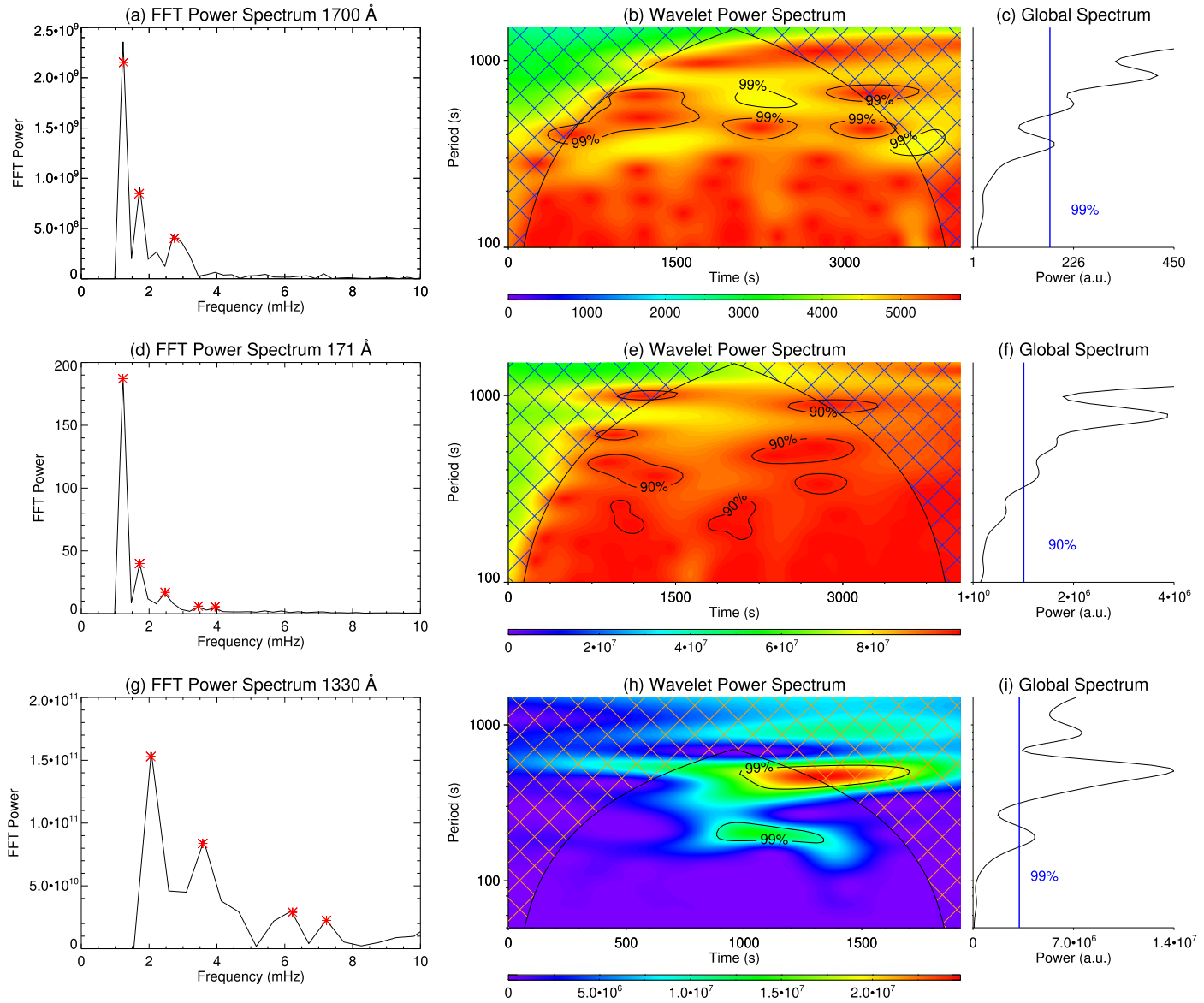

Figure 2. FFT power spectrum as a function of frequency (mHz) for 1700 Å (a), 171 Å (d), and 1330 Å (g) wavelengths. Peaks highlighted with the red asterisks indicate the dominant frequencies present in the signal. The middle column shows the wavelet power as a function of period and time. The confidence level greater than 90% are enclosed by black contours. The right column shows the corresponding global spectrum.

(g) the peaks marked are at 3, 4, and 8 minutes. The middle column shows the wavelet power spectrum for 1700 Å (b), 171 Å, (e), and 1330 Å (h), respectively. Outside the Cone of Influence, it is possible to identify periods 6, 9, and 13 minutes enclosed by black contours with the 99% confidence level in 1700 Å, which is confirmed by the blue line over the global spectrum in the right column (panel (c)). In the same way for 171 Å (e), the periodicities seen in the power FFT spectrum are enclosed with the 90% confidence level in the power wavelet spectrum and the same peaks are over the 90% significance level in the global spectrum (panel (f)). Note that 3 and 8 minutes periodicities with 99% of the significance level are seen in power and global spectra computed for 1330 Å (panels (h–i)). The presence or the absence of 13 minute oscillation could not be verified in 1330 Å wavelength data due to the spatial and temporal limitation of the data.

We also used the Pixelised Wavelet Filtering (PWF) method (Sych & Nakariakov 2008) in order to identify the spatial distribution of periodicities present in various ROIs. The PWF method is based on calculating the wavelet transform over the time signal of each pixel inside the chosen ROI. We then obtained the temporal signal filtered by predominant period bands. These period bands were chosen as 2–3 minutes, 3–5 minutes, 5–7 minutes, 7–12 minutes, 12–14 minutes, which we will now refer to by their central periods 2.5, 4, 6, 9, 13 minutes, respectively. The spatial distribution of powers for each filtered period band is computed and the movies of narrowband maps $\geqslant$4 minutes are provided (movies m4m.mp4, m6m.mp4, m9m.mp4 are available in the tar.gz package).

3. Results

3.1. Detected Periodicities

The intensity oscillations in *SDO*/AIA 171 Å passband were obtained for a low-lying coronal arcade in the vicinity of the flaring site. We found oscillations of 4, 6, 9, and 13 minutes,

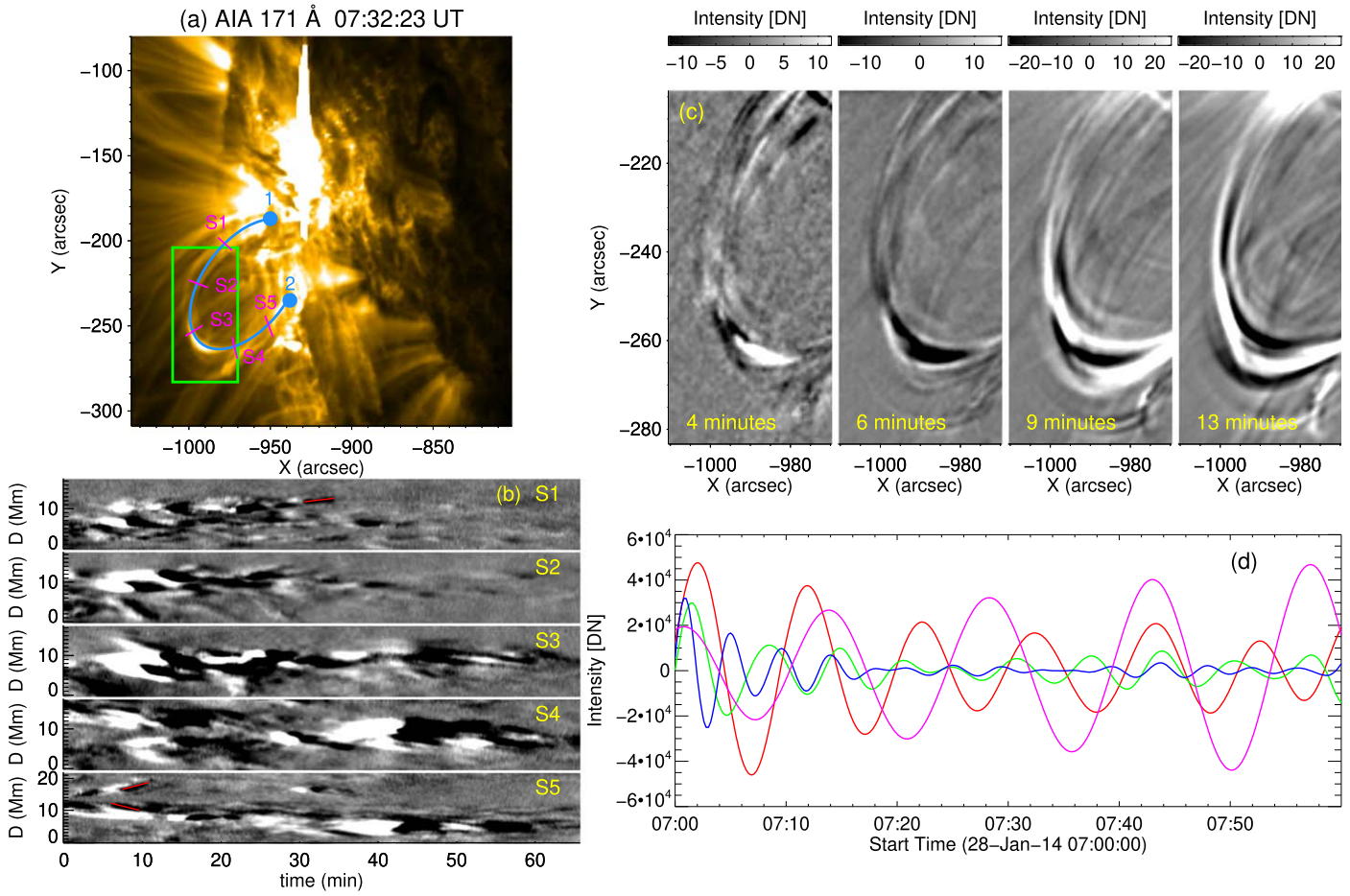

Figure 3. Oscillations found in the top of the coronal loops observed in *SDO*/AIA 171 Å. (a) EUV snapshot of the coronal loops as observed in *SDO*/AIA 171 Å passband. The loop shape and its endpoints are shown in blue color. (b) Distance–time maps made for each purple slit traced across the loop in panel (a). Disturbance speed was calculated over the slits S1 and S5, which are represented by red lines. (c) Filtered intensity maps for oscillations of 4, 6, 9, and 13 minutes seen in the loop-tops region shown in (a). (d) Filtered integrated intensity variation as a function of time for the maps shown in (c). Lines blue, green, red, and purple correspond to oscillations of 4, 6, 9, and 13 minutes, respectively.

along the coronal loop structure in 171 Å images. The intensity variations are in phase suggesting the presence of standing oscillations.[7]

Figure 3 shows periodicities of 4, 6, 9, and 13 minutes detected in the loop-tops in 171 Å channel of *SDO*/AIA. In panel (a), the green box highlights the region where the oscillations were found. To investigate further, we first define the loop structure and then study the oscillations at various locations along this defined loop. This fitted loop, as well as the endpoints, are overplotted in blue color. We traced five equally spaced slits, in purple color, across the loop; four of them chosen to be 41 pixels long (≈18 Mm) and 5 pixels wide. The slit number 5 was 51 pixels long (≈22 Mm) in order to see more details of the disturbances close to the endpoint 2. To increase the signal-to-noise ratio we calculated the average intensity over the slit width (Anfinogentov et al. 2013). Then we created time-distance maps with 2 minutes running difference images (Wang et al. 2009), which show propagating and standing modes in the loops (see Figure 3(b)). Figure 3(c) shows the spatial distribution of the filtered signal for the detected periodicities. Note that the bright and dark color indicate variations in the intensity of the filtered signal within each band. In Figure 3(d), we display the filtered signal integrated for each narrowband map shown in Figure 3(c). The periodic behavior can be clearly seen in the curves in blue (4 minutes), green (6 minutes), red (9 minutes), and purple (13 minutes) colors. Most oscillations show decaying nature prior to the flaring except for the 13 minute oscillation, which has a slightly growing amplitude. It is possible that during the flaring activity, more external energy is fed to the loop-top and the oscillation with relatively longer period such as the 13 minute oscillation here continues to grow in amplitude for a while.

From the slit 1, we can see that close to the endpoint 1, there are propagating waves, before the flare, with velocities of 3.82 km s^{-1}. At the top of the loops, the disturbances are present throughout the duration of our observation (see slit S3). However, in slit 4 the disturbances are located in two different places during the first 30 minutes. After the flare begins, the disturbances are seen in the center of the slit with an increased amplitude. Slit 5, located near the endpoint 2, shows two different period-modes propagating with velocities of 10.67 and 10.08 km s^{-1} in opposite directions. Oscillations close to endpoint 2 and the top of the loops were seen throughout the one hour duration (see slits S3, S4, and S5), while near to point 1 the disturbances were seen before the flare begins.

We estimated the length (L) of the loop shown in Figure 3(a) by fitting an ellipse over points traced in the bright part of the set of loops (see, for example, Anfinogentov et al. 2013). Then,

[7] The movies of narrowband phase maps (phase4m.mp4, phase6m.mp4, phase9m.mp4, and phase13m.mp4) are available in the tar.gz package.

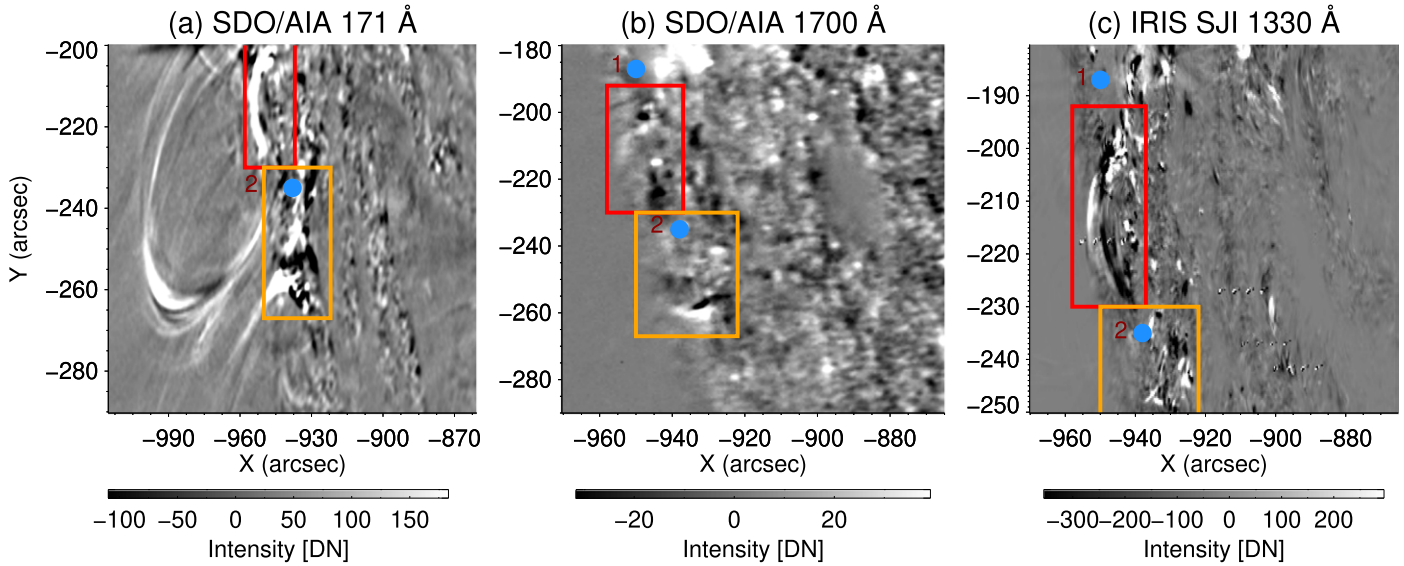

Figure 4. Filtered intensity map in the narrowband centered in 6 minutes, detected simultaneously in (a) *SDO*/AIA 171 Å, (b) *SDO*/AIA 1700 Å, and (c) *IRIS* SJI 1330 Å. The red box shows the spatial coincidence in the oscillations observed between the endpoints of the loops seen in 171 Å (Figure 1 (a)). The orange box represents another common region between the three wavelengths. The endpoints are denoted by the blue filled circles.

we calculated the phase speed, $v_{\rm ph} = L/P$, for each period (P) detected from the PWF method. The fitted loop has a length of $L = 117{,}282$ km ≈ 117 Mm. Thus, the $v_{\rm ph}$ for the oscillations of 4, 6, 9, and 13 minutes were 488, 325, 217, and 150 km s^{-1}, respectively.

On the other hand, considering the temperature response $T_e = 6.3 \times 10^5$ K for AIA 171 Å instrument (Lemen et al. 2012), to calculate the approximate sound speed $c_s = 147\sqrt{T_e/10^6}$ km s^{-1} (Aschwanden 2004) we obtain 116.67 km s^{-1}. The values of these speeds suggests that these are likely to be slow magnetoacoustic modes (Aschwanden 2004; Wang et al. 2009) although a definite confirmation requires simultaneous Doppler velocity data, which unfortunately is unavailable. The filtered signal in Figure 3(d) shows a decaying profile for oscillations of 4, 6, and 9 minutes around the flaring time but non-decaying for 13 minutes.

Standing oscillations of 4, 6, 9, and 13 minutes are also seen in 1700 Å data, in the vicinity of the endpoints of the loops. Similarly, standing modes of 3, 4, and 8 minutes are observed in SJI-1330 Å wavelength, between the endpoints of the loop structure. Movies of the phase maps are available in the tar.gz package. Although the power is dominant at some discrete frequencies, there is substantial power at other frequencies too. As an example, in Figure 4 we show oscillations of 6 minutes detected in 171 Å, 1700 Å, and SJI 1330 Å. The red box shows the spatial overlap in the oscillations observed between the endpoints of the loops seen in 171 Å (Figure 3). The orange box represents another common point (endpoint 2) between the three wavelengths.

3.2. Doppler Velocity

The movie (o1700pf.mp4) created using AIA 1700 Å images also clearly show the 3D vortices near endpoint 1. In particular, the filtered intensity maps of 4, 6, and 9 minute periodicities show strong bright and dark features swirling around near the endpoint 1. They match spatially and temporarily with the eruptions and jets showed in ar2.mp4 and ar304.mp4, described in Section 2. Therefore, the resulting upflows and downflows should be visible in the line-of-sight Doppler velocity maps.

We studied the Doppler velocities for the *IRIS* spectral data. In order to obtain the dopplergrams, we considered the velocity shift in ±50, ±20, and ±40 km s^{-1} from the Mg II k 2796 Å, C II 1336 Å, and Si IV 1403 Å core spectral lines, respectively. We used the dopplergrams from 7:30 to 8:07 UT and the convention that the negative velocities are for upflows.

In Figure 5 panel (a) we show the oscillations of 13 minutes found in AR 11967 in *SDO*/AIA 171 Å (black contour) and 1700 Å (orange contour) data, around the coronal loops as an example. We indicate the positions of the endpoints with blue filled circles; note that endpoint 1 is close to a sunspot seen from Helioseismic and Magnetic Imager (HMI; see Scherrer et al. 2011) on board *SDO* and overlapped with a pink contour. We also overplot the location of 6 minute oscillations as detected in the *IRIS* SJI 1330 Å data with green contours. In panels (b–d) we show the Doppler velocities for Mg II k 2796 Å, C II 1336 Å, and Si IV 1403 Å, respectively.[8] The FOV of these dopplergrams is indicated with an aquamarine box over the image in panel (a). The distance between the endpoints and the SG FOV is around 26″ (1) and 14″ (2), which is equivalent to 11 Mm and 6.1 Mm, respectively. These distances may seem large, but we reckon that if *IRIS* had a bigger FOV for this raster data, we would have been able to track the upflows all the way up to the location of the endpoints.

In Mg II k 2796 Å line, the flow appears to be toward the endpoint 2, where the variation of intensity was most intense (see Figure 5(a)). Contrary to this, a flow appears to be moving away from endpoint 1, which was close to the flare site (see Figure 1(a)).

4. Discussion and Conclusions

We carried out a time-series analysis of a coronal arcade lying low on the southeastern limb of the Sun. The arcade-top

[8] Movies about dopplergrams are available in the tar.gz package.

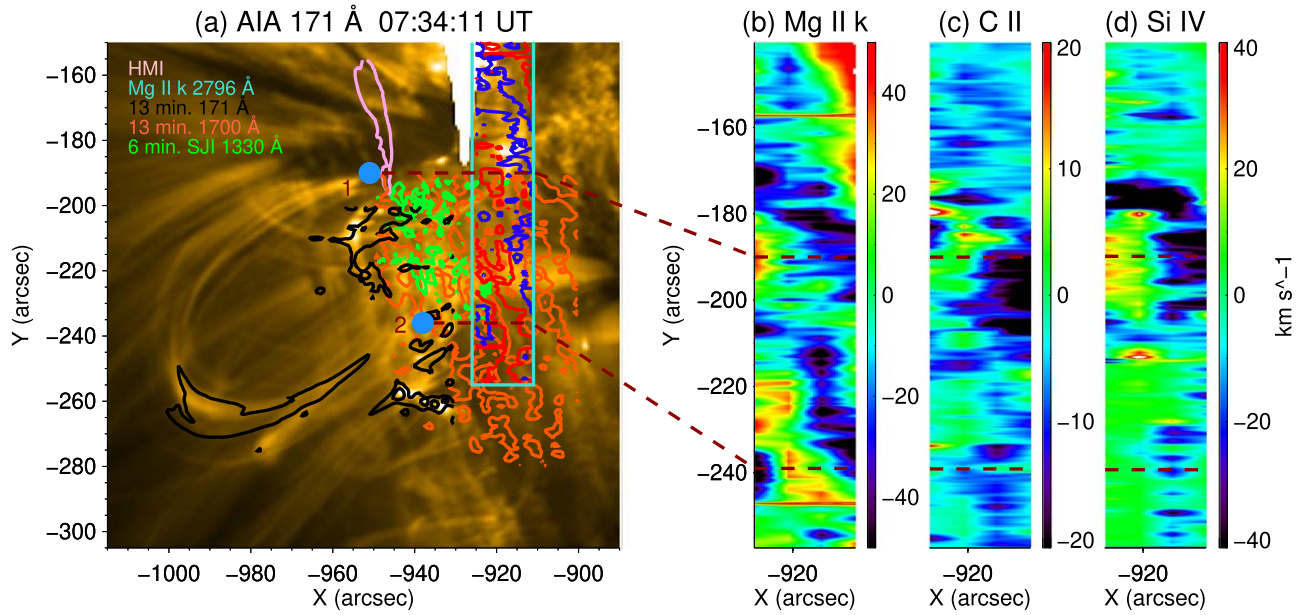

Figure 5. (a) Coronal loops of AR 11967 as seen in *SDO*/AIA 171 Å and spatial location of the oscillations found in the loops. The pink contour represents the sunspot position seen from the HMI instrument (Scherrer et al. 2011) and blue filled circles show the position of the endpoints of the loops. Oscillations of 13 minutes observed in *SDO*/AIA 171 Å and 1700 Å are indicated by the black and orange contours, respectively. We also show, for comparison, the 6 minute oscillations as detected in SJI-1330 Å by green contours. The aquamarine box encloses the FOV of the dopplergram for the Mg II k 2796 Å spectral line. The blue color means negative velocities showing up-flow, and red represents the opposite. The dashed lines connect the position of the endpoints with the dopplergram overlapped in panel (a) and with more details in panel (b). Panels (c) and (d) show dopplergrams for C II 1336 Å and Si IV 1403 Å, respectively.

showed intensity variations of 4, 6, 9, and 13 minutes in *SDO*/AIA 171 and 1700 Å passbands. The analyzed time series includes the time when an M3.6 flare was recorded in X-ray flux by the *GOES*-15 instrument and other eruptions seen in *SDO*/AIA 1700, 304, 171, and *IRIS* SJI 1330 Å images. The time-distance maps, created using various slits across the loops, show disturbances in the loops either for partial or for the entire duration of the observational time. Some oscillations are seen before the flare in a region close to endpoint 1. After the flare, the legs of some of the loops closer to endpoint 2 were pushed together and larger period oscillations continue to grow slightly in amplitude. The oscillations with 9 minutes periodicity as the dominant one before the flaring and 13 minutes as the dominant one immediately after the flaring are also seen clearly in the filtered intensity signal (refer to Figure 3(d)). It is likely that the flare supplied more energy at the loop-top (at the coronal height), which enhanced the amplitude of the 13 minute oscillation for a while, as seen in 171 Å wavelength. A clear presence or absence of 13 minute oscillation in *IRIS* SJI 1330 Å data could not be confirmed because of the restricted amount of data both temporally and spatially.

Based on the maps created with *IRIS* SJI 1330 Å data and *SDO*/AIA 1700 Å data, movies of different wavelength data for the spatially aligned ROI, and using *IRIS* dopplergrams in Mg II k, C II, and Si IV, we suggest that the excitation sources of oscillations are in the lower atmosphere and the flare provided appropriate condition in coronal plasma that enhanced the power and enabled us to detect a discrete dominant periodicity of 13 minute in 171 Å AIA/*SDO* wavelength passband.

We have identified the approximate spatial location of the perturbations in the lower regions of the solar atmosphere, from where disturbances may have propagated upward and triggered the oscillations in the loop structure of the coronal arcade, as observed by intensity variations in the loop structure in *SDO*/AIA 171 Å images (see Figure 3). As demonstrated in Figure 5, these disturbances have their origin in the lower layers, where the endpoints of the coronal loop structure are presumably anchored. In particular, endpoint 1 is close to a sunspot (see Figures 1(b) and 5(a)) and could be perturbed by the excitation sources in these layers. Note that after allowing for small errors, the periodicities of the detected oscillations is close to higher harmonics of the 3 minute oscillations that are often detected in sunspots. Such a relationship between a sunspot and flare-induced oscillations in an active region have been previously reported by Sych et al. (2009) while investigating microwave light curves of the flares. They showed possible leakage of 3 minutes oscillations from the sunspot into the active region before and during the flaring activity. Prior to this study, Zaĭtsev & Kislyakov (2006) also observed three signals with periods 3.3, 5, and 10 minutes suggesting parametric resonance between 5 minute p-modes and natural acoustic oscillations of coronal loops.

Another possible sources of excitation in our data set are the jet-like features or the swirls near the endpoints at lower layers and/or the strong eruptions accompanying a flaring activity seen in the lower regions. The signature of ∼4, ∼6, and ∼9 minute periodicities can be clearly seen near the endpoints in the movies created with images obtained in *SDO*/AIA 1700 Å and *IRIS* SJI 1330 Å lines. The corresponding upflows and downflows in the Doppler velocity maps obtained by *IRIS* in Mg II k, C II, and Si IV also support the scenario that there were perturbations in the area where endpoint 1 was probably anchored. Disturbances associated with transient flows periodically ejected at the footpoint are not uncommon. They have been detected previously in fan-like coronal loops by Berghmans & Clette (1999) and revealed as slow magnetoacoustic waves propagating upward (see, for example, Wang et al. 2009 and Verwichte et al. 2009). A jet-like feature near endpoint 2 at the

time of flaring activity may have also contributed to the oscillations seen in the slits S4 and S5.

S.M.C.C. acknowledges financial support from the São Paulo Research Foundation FAPESP (grant No. 2018/25306-9). R.J. is grateful to MSRC (University of Sheffield, UK) for funding S.M.C.C.'s research visit to the University of Sheffield. V.J.-P. thanks FAPESP (grant No. 2013/10559-5) for support. Thanks are also extended to the NASA/*SDO*, the AIA, the HMI, and *GOES* science teams. *IRIS* is a NASA small explorer mission developed and operated by LMSAL with mission operations executed at NASA Ames Research center and major contributions to downlink communications funded by ESA and the Norwegian Space Centre.

ORCID iDs

Rekha Jain https://orcid.org/0000-0002-0080-5445
Vera Jatenco-Pereira https://orcid.org/0000-0002-1517-0710

References

Allian, F., Jain, R., & Hindman, B. W. 2019, ApJ, 880, 3
Anfinogentov, S., Nisticò, G., & Nakariakov, V. M. 2013, A&A, 560, A107
Aschwanden, M. J. 1994, SoPh, 152, 53
Aschwanden, M. J. 2004, Physics of the Solar Corona (Chichester: Praxis)
Aschwanden, M. J., Fletcher, L., Schrijver, C. J., & Alexander, D. 1999, ApJ, 520, 880
Aschwanden, M. J., & Schrijver, C. J. 2011, ApJ, 736, 102
Berghmans, D., & Clette, F. 1999, SoPh, 186, 207
Conde, C. S. M., Costa, J. E. R., & Cedeño, M. C. E. 2016, SoPh, 291, 3289
DePontieu, B., Title, A. M., Lemen, J. R., et al. 2014, SoPh, 289, 2733
Jain, R., Maurya, R. A., & Hindman, B. W. 2015, ApJL, 804, L19
Kumar, P., Nakariakov, V. M., & Cho, K.-S. 2016, ApJ, 822, 7
Kupriyanova, E. G., Melnikov, V. F., Nakariakov, V. M., & Shibasaki, K. 2010, SoPh, 267, 329
Lemen, J. R., Title, A. M., Akin, D. J., et al. 2012, SoPh, 275, 17
Nakariakov, V. M., Foullon, C., Myagkova, I. N., & Inglis, A. R. 2010, ApJL, 708, L47
Nakariakov, V. M., Ofman, L., Deluca, E. E., Roberts, B., & Davila, J. M. 1999, Sci, 285, 862
Pesnell, W. D., Thompson, B. J., & Chamberlin, P. C. 2012, SoPh, 275, 3
Rathore, B., Carlsson, M., Leenaarts, J., & De Pontieu, B. 2015, ApJ, 811, 81
Scherrer, P. H., Schou, J., Bush, R. I., et al. 2011, SoPh, 275, 207
Sych, R., Nakariakov, V. M., Karlicky, M., & Anfinogentov, S. 2009, A&A, 505, 791
Sych, R. A., & Nakariakov, V. M. 2008, SoPh, 248, 395
Torrence, C., & Compo, G. P. 1998, BAMS, 79, 61
Verwichte, E., Aschwanden, M. J., Van Doorsselaere, T., Foullon, C., & Nakariakov, V. M. 2009, ApJ, 698, 397
Wang, T. J., Ofman, L., Davila, J. M., & Mariska, J. T. 2009, A&A, 503, L25
Zaĭtsev, V. V., & Kislyakov, A. G. 2006, ARep, 50, 823